M&C 2017 - International Conference on Mathematics & Computational Methods Applied to Nuclear Science & Engineering, Jeju, Korea, April 16-20, 2017, on USB (2017)

Impact of Photon Transport on Power Distribution

LIEGEARD Clément[*†], CALLOO Ansar[*], MARLEAU Guy[†], GIRARDI Enrico[*]

[*] *Électricité de France, R&D, Simulation neutronique techniques de l'information et calcul scientifique*
[†] *Institut de génie nucléaire - Polytechnique Montréal*
clement.liegeard@polymtl.ca, ansar.calloo@edf.fr, guy.marleau@polymtl.ca, enrico.girardi@edf.fr

Abstract - *Present reactor calculation chains consider that the energy of the photons is deposited locally whereas the photons are actually transported and have a significant impact on the power distribution. Photons (mainly gamma photons) have particularly an impact on the hot spot of nuclear elements. This work extends existing neutron lattice calculation schemes to neutron-gamma lattice calculation schemes and explains in detail the impact of gamma transport on different power maps of PWR.*

I. INTRODUCTION

EDF R&D is responsible for the conception of tools used for modeling the physical phenomena occurring in the nuclear reactor core. As far as the neutronic simulations are concerned, the calculation chain currently used in the operational and the engineering divisions is called CASSIOPEE. Nevertheless, EDF R&D has been working on the conception of a new, state-of-the-art calculation chain, ANDROMEDE, that will replace the one in operation in a few years. This new neutronic calculation chain consists of two distinct parts: lattice/assembly calculations are carried out by the transport code APOLLO-2 [1] developed by the French atomic commission - *Commissariat à l'Énergie Atomique et aux Énergies Alternatives* (CEA) with the financial support of EDF and AREVA. Core calculations are performed using the 3D core code COCAGNE which is developed at EDF R&D. The lattice calculations are based on the REL-2005 scheme [2] coupled with the CEA nuclear data library CEA2005v4 based on JEFF 3.1.1 nuclear data evaluations. This scheme is an optimised version of the SHEM-MOC scheme used as a reference for assembly depletion. Both schemes have been validated extensively by the CEA.

In recent years, coupled neutron-gamma calculations have become more and more prevalent in modern computation chains. For example, the lattice code CASMO-5 implemented gamma libraries [3] and AREVA started to perform gamma calculations for safety reports [4]. Gamma transport is important as it is a physical phenomenon which actually takes place in the nuclear reactor and may have several impacts. It may, in particular, change the power distribution of a core [5] and affect the temperature and the spatial location of the hot spot in the core. On the other hand, gamma transport increases the calculation time and thus its effects have to be studied before being added in industrial calculation chains.

In this work, we extend both the SHEM-MOC and REL-2005 schemes to neutron-gamma transport schemes to be able to compute the energy deposited in various parts of the lattice from both neutrons and gamma particles. At the moment, the SHEM-MOC and REL-2005 schemes do not transport photons. Therefore, the energy released by a gamma is deposited at its birthplace: whereas the gamma, in fact, interacts with nuclides generally located at a different spatial position.

In this work, after a short description of differences between the two APOLLO-2 calculation schemes considered, the validation of the deterministic gamma transport scheme in assemblies is performed with the help of TRIPOLI-4 [6, 7]. The calculations from this code are used as a reference for fresh assemblies as it uses the Monte-Carlo method and it performs truly coupled neutron-photon calculations. For depletion studies, we use the SHEM-MOC scheme as a reference for both neutron and gamma calculations. Then the impact of the gamma transport on the power distribution map in an assembly is described before studying larger structures.

II. NEUTRON-PHOTON DETERMINISTIC SCHEMES

Three deterministic schemes are used: the SHEM-MOC-gamma is our reference; the REL-94 has relaxed neutron transport options and is used as an intermediate step between the 2 other schemes to evaluate the effects of relaxing the neutron transport options on the gamma flux; the REL-2005-gamma has relaxed neutron and photon transport options and is the optimized scheme. For gamma transport, we used the CEAV5.1.2 library based on JEFF3.1.1 nuclear data evaluations. Contrarily to the Monte-Carlo reference that uses coupled neutron-gamma, our deterministic schemes are chained neutron-gamma calculations. The gamma transport calculations have no effect on the neutron calculations. Moreover, every scheme gives the 18-group photon flux for each cell and the power deposited in each cell. In this manner, it is possible to directly compare the three schemes.

The order of anisotropy for the gamma transport did not create significant differences in the flux results. However, since we only want to study the gamma transport effects, the calculation time is not an obstacle and, generally, we choose to have the maximum order of anisotropy for our calculations. All the calculations shown in this paper come from gamma transport with a P5 order of anisotropy.

1. SHEM-MOC-gamma

Here we present the different steps of the SHEM-MOC-gamma calculation:

- Single-level neutron transport: 281 energy groups in a refined mesh (RAF mesh, see Fig. 1) using the method of characteristics (MOC).
- Creation of the 94-group photon sources on the RAF mesh with a production matrix: 281 neutron groups to 94

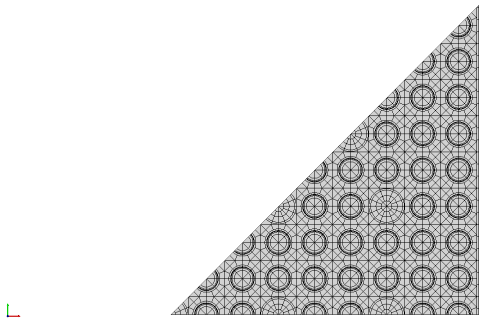

Fig. 1. RAF mesh: refined geometry mesh on an eighth of assembly.

photon groups.

- Single-level MOC based photon transport: 94 energy groups on the RAF mesh.

The SHEM-MOC-gamma is the most precise deterministic neutron and gamma transport calculation we performed. The 2 other schemes below have a lower accuracy due to coarser energy and geometry meshes.

2. REL-94

- REL-2005 [2] is a two-level scheme :
  - 281 energy groups on a coarse geometry mesh using the collision probability (CP) method.
  - Collapsing the neutron flux to 26 groups and transport on a MAV mesh (windmill ("moulin-à-vent") mesh, see Fig. 2) using the MOC.

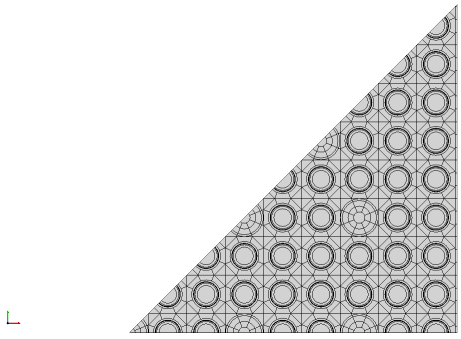

Fig. 2. MAV mesh: intermediate geometry mesh on an eighth of assembly.

- Reconstruction of a 281-group neutron flux and creation of the 94-group photon source with the production matrix. As we only have a 281*94 matrix provided by the CEA to create the photon source, the neutron flux has to be reconstructed on our mesh at 281 groups. In order to achieve this, the homogenized 281-group flux coming from the first level of calculation and the 26-group flux on the MAV mesh are used.
- Single-level MOC based photon transport: 94 energy groups on the MAV mesh.

The gamma transport increases the calculation time by a factor between 2 and 3 depending on the order of anisotropy. This scheme has the highest relative calculation time increase because we only transport 26 neutron groups on the MAV mesh against 94 gamma groups on the same mesh. However, the modules used in the gamma part of the scheme were not optimized as we use a development version of APOLLO-2 and we did not invest efforts in reducing the calculation times.

3. REL-2005-gamma

- REL-2005 is a two-level scheme :
  - 281 energy groups in a coarse geometry mesh using the CP method.
  - Collapsing the neutron flux to 26 groups and transport on a MAV mesh using the MOC.
- Reconstruction of the 281-group neutron flux and creation of the 94-group photon source with the production matrix. This is followed by a condensation of the gamma source to 18 groups.
- Single-level MOC based photon transport: 18-group photon transport on the MAV mesh.

The effects of the photon transport on three different assemblies are investigated: UOX (uranium oxides), MOX (plutonium and uranium oxides) and UOX-Gd (UOX assembly with burnable poison pins). All the assemblies have 17*17 cells. The UOX assembly is only composed of pins made of enriched uranium. The MOX assembly contains three types of MOX pins at different enrichments (see Fig. 3). The UOX-Gd is composed of UOX pins some of which also contain gadolinium. In this work, we mainly focus on the MOX assembly.

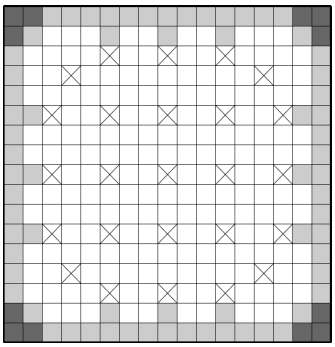

Fig. 3. MOX assembly, the crosses represent the cells without fuel (guide thimbles). The highly enriched pins are white, intermediate pins are slightly shaded, low enriched pins are dark.

4. Validation of the schemes

First of all, the SHEM-MOC results are compared to TRIPOLI-4 for fresh assemblies. Thus, flux differences are calculated as:

$$\text{Difference} = \frac{\text{Flux} - \text{Flux}_{\text{reference}}}{\text{Flux}_{\text{reference}}} * 100 \quad (\%) \qquad (1)$$

Fig. 4 shows the differences for the pin-by-pin photon flux collapsed to 1 group between TRIPOLI-4 and the SHEM-MOC-gamma. These differences are lower than 0.25% and the root mean square (RMS) is equal to 0.09% which is very low.

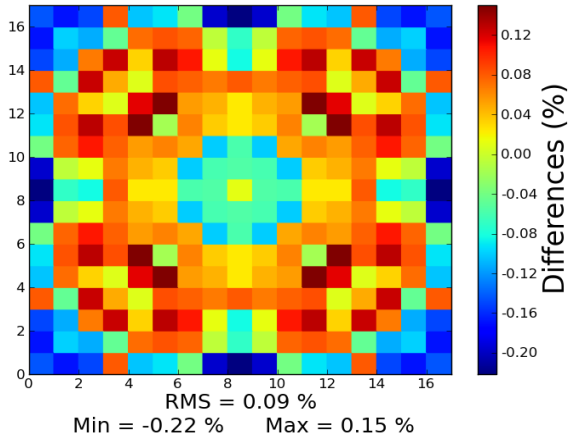

Fig. 4. Photon flux (collapsed to 1 group) differences between the SHEM-MOC-gamma and the TRIPOLI-4 reference on a fresh MOX assembly. RMS = root mean square

When we compare the 18-group photon flux, it appears that in most cases, the differences don't exceed 1%. For the groups at the highest energy and the lowest energy, differences can reach few percents. Those differences come from the fact that the flux is almost 100 times lower in those groups than in the other and thus the relative differences increase substantially.

For the other two assemblies (UOX and UOX-Gd) the differences are of the same order of magnitude. As our SHEM-MOC-gamma scheme shows good results for three different fresh assemblies, we assume that it is validated for the gamma transport.

As the gamma calculation doesn't affect the neutron calculation in our schemes, the validated micro-depletion scheme of SHEM-MOC remains valid and so does ours.

The SHEM-MOC-gamma is then used for depletion calculations as a reference for the other schemes (REL-94 and REL-2005-gamma). At $t = 0$, the gamma flux collapsed to 1 group obtained with the REL-94 or the REL-2005-gamma are very similar to those calculated with the SHEM-MOC-gamma. Indeed, differences lower than 1% for each cell appear and the root mean square is equal to 0.31% for the comparisons with the REL94 and to 0.25% for the comparisons with the REL-2005-gamma (see Fig. 5 for differences between the SHEM-MOC-gamma and the REL94 and Fig. 6 for differences between the SHEM-MOC-gamma and the REL-2005-gamma).

Here, the root mean square is slightly lower in the case of the REL-2005-gamma while this scheme should show less accuracy due to the coarser calculation options. More generally, for other burn-ups and other assemblies, the REL94 and the

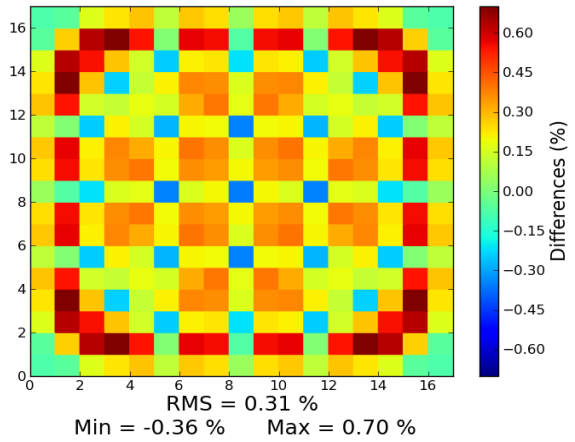

Fig. 5. Photon flux (collapsed to 1 group) differences between the REL94 and the SHEM-MOC-gamma on a fresh MOX assembly.

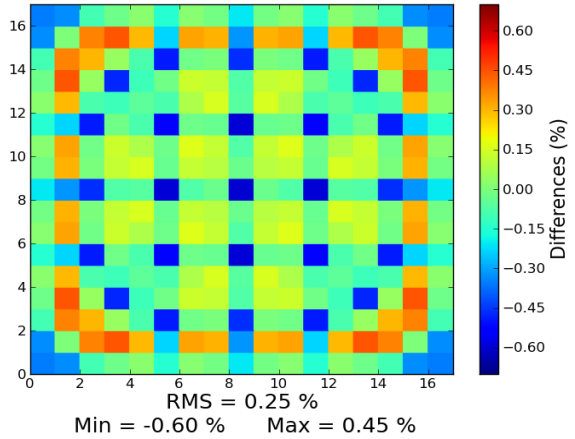

Fig. 6. Photon flux (collapsed to 1 group) differences between the REL-2005-gamma and the SHEM-MOC-gamma on a fresh MOX assembly.

REL-2005-gamma schemes provide very similar results.

Furthermore, the differences between the gamma flux calculations is almost constant during depletion.

As a result, the total power (neutrons and photons) differences stay below 1% for fuel cells for the whole depletion calculations (see Fig. 7, for differences between the REL-2005-gamma and the SHEM-MOC-gamma). The guide thimbles have a different behavior : the relative power differences between schemes reaches 12%. Since the power deposited there is more than one order of magnitude lower than in the fuel cells, the impact of these higher differences can be neglected (see Fig. 8). Very similar results are also observed for the UOX and UOX-Gd assemblies.

In conclusion, the low differences for gamma flux calcu-

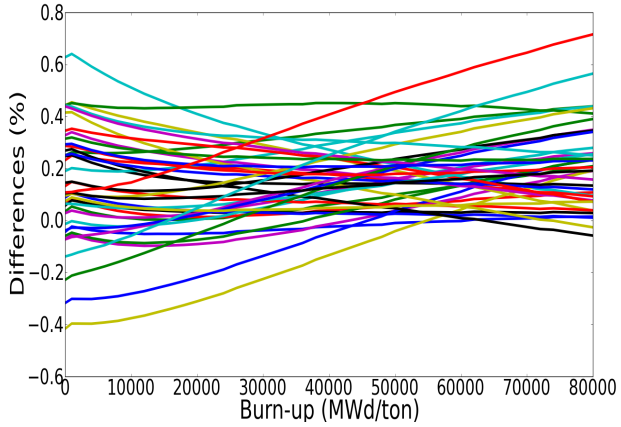

Fig. 7. Total power differences between the REL-2005-gamma and the SHEM-MOC-gamma for an eighth of the MOX assembly. Each curve represents a fuel cell

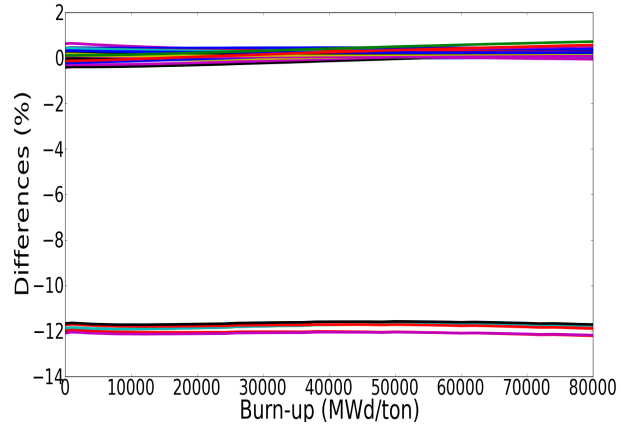

Fig. 8. Total power differences between the REL-2005-gamma and the SHEM-MOC-gamma for an eighth of the MOX assembly. Each curve represents a cell, the cells that have the differences around -12% are the guide thimbles

lations and power deposited calculations validate the use of our three schemes.

Now the differences brought by the gamma transport on the power map will be described.

III. IMPACT OF THE PHOTON TRANSPORT ON THE POWER DISTRIBUTION

The gamma transport does not affect the total power deposited on the assembly, it only affects locally the power map. Moreover, the global shapes of the power map are very similar with and without gamma transport.

In this section, we still mainly focus on the MOX assembly. Unless mentioned otherwise, the power map is normalized at $38.961 W/g$. Moreover, the power maps are obtained with SHEM-MOC(-gamma) calculations with a P5 order of anisotropy for photons.

1. Assembly calculations

With three different enrichments in the fuel of the fresh MOX assembly, the power deposited in the fuel varies substantially between the cells. Fig. 9 shows the power map after gamma transport where highly enriched pins reach $\simeq 1.28 MeV/s$ while low enriched pins only reach $\simeq 0.84 MeV/s$. Accordingly, the power deposited is much greater in the central pins than in the peripheral pins.

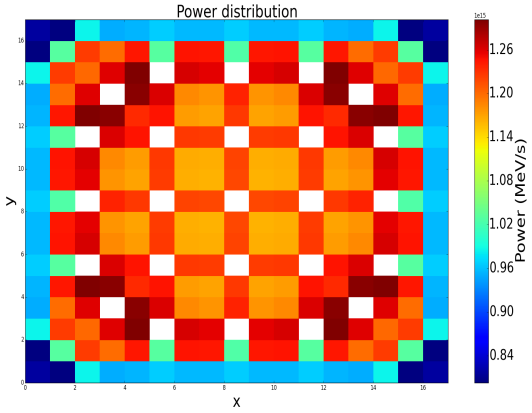

Fig. 9. Power distribution in a fresh MOX assembly (results with photon transport).

After every calculations, the impact of the gamma transport is calculated as follows:

$$\text{Difference} = \frac{P_{ng} - P_n}{P_n} * 100 \quad (\%) \tag{2}$$

where P_{ng} is the power distribution from a neutron-photon calculation and P_n the power from an only-neutron calculation.

For a fresh MOX assembly, the photon transport increases the power deposited in the low enriched pins by up to 2.44% while we observe a decrease around 0.8% in the highly enriched pins (see Fig. 10). Indeed, the highly enriched pins emit more photons than the other and each pin absorbs a similar fraction of the photon flux. Therefore, low enriched pins (and intermediate pins) will absorb more photons energy than they emit and thus the gamma transport increases the power deposited in those cells.

For the fuel cells, the root mean square is equal to 0.79% so the gamma transport has significant effects on the power distribution.

The guide thimble cells do not emit photons at all but do absorb them. Indeed, the moderator is not a significant gamma source. Therefore, the power deposited in these cells will greatly increase ($\simeq 65\%$, see Fig. 11).

Moreover, as explained before, the power deposited in those cells is very low. Therefore, the total power deposited in the water is still very low compared to the total power deposited in the fuel and guide thimbles won't be studied in the remaining sections of this work. This effect can particularly be

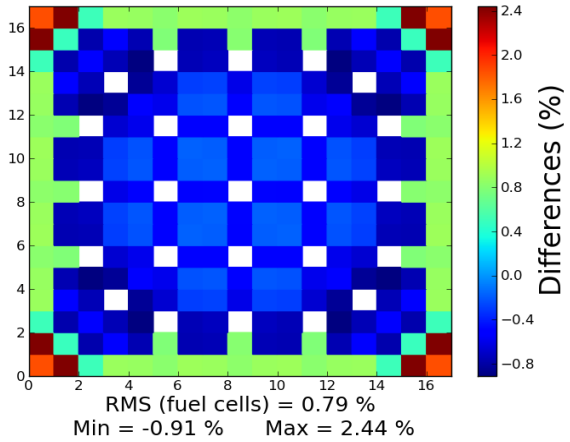

Fig. 10. Cell by cell relative power differences obtained with photon transport in a fresh MOX assembly. Guide thimbles are out of the color scale.

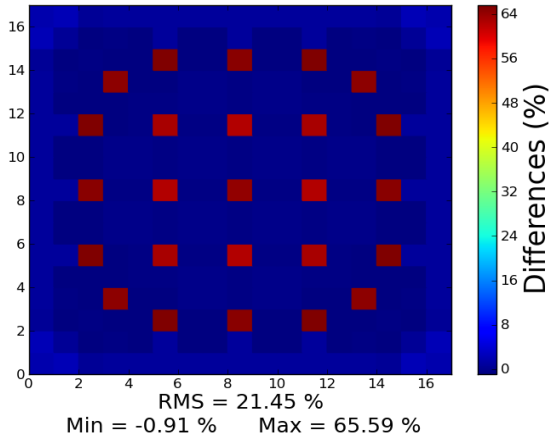

Fig. 11. Cell by cell relative power differences (included guide thimbles) obtained with photon transport in a fresh MOX assembly.

seen when we compare each material (fuel, water/moderator, cladding) on Fig. 12 : the power deposited in the moderator increases by 27.3%. Moreover, on the same figure, we note that the photons have an impact on the claddings similar to the moderator. The cladding isn't a significant source of photons, nevertheless it absorbs a part of the gamma flux and the power deposited in the cladding will be considerably larger (+344%).

During depletion, the shape of the difference map does not vary substantially. Nevertheless, the power deposited in the highly enriched pins gets closer to the power deposited in the less enriched pins and thus, the differences brought by the photon transport tend to decrease. At a burnup of $20GWd/ton$, the root mean square reaches 0.73% and at $60GWd/ton$, it only reaches 0.58%, compared to the 0.79% we had for the fresh assembly (see Fig. 13 and Fig. 14).

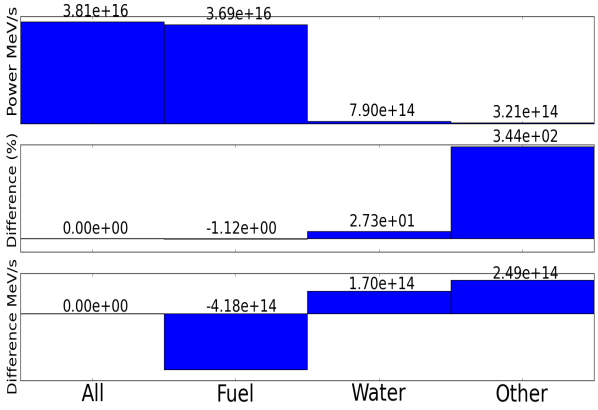

Fig. 12. Impact of the gamma transport on each environment (fuel, moderator, cladding). The top figure, shows the power deposited. The center figure shows the relative impact of the gamma transport. The bottom figure shows the absolute impact of the gamma transport.

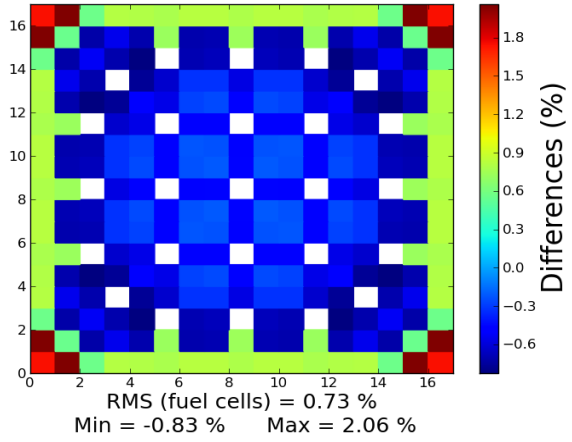

Fig. 13. Cell by cell relative power differences obtained with photon transport in a MOX assembly at $20GWd/ton$. Guide thimbles are out of the color scale.

Finally, for the MOX assembly the gamma transport will smooth down the power distribution with differences in the fuel cells of the order of 1%. Bigger structures have to be studied to evaluate first the impact of the environment of the assembly on the gamma transport and then the impact of the gamma transport on the hot spot of a core.

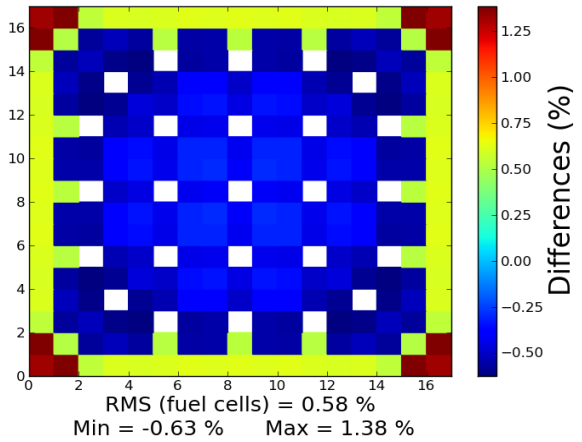

Fig. 14. Cell by cell relative power differences obtained with photon transport in a MOX assembly at $60GWd/ton$. Guide thimbles are out of the color scale.

In the UOX assembly, each pin has the same composition at $t = 0$. Therefore, the impact of the gamma transport is clearly less significant than in the MOX assembly. For example, the maximum difference obtained with photon transport on the fuel cells of a UOX assembly is only 0.35% (see Fig. 15). During depletion, the impact of the gamma transport decreases as observed before for the MOX assembly.

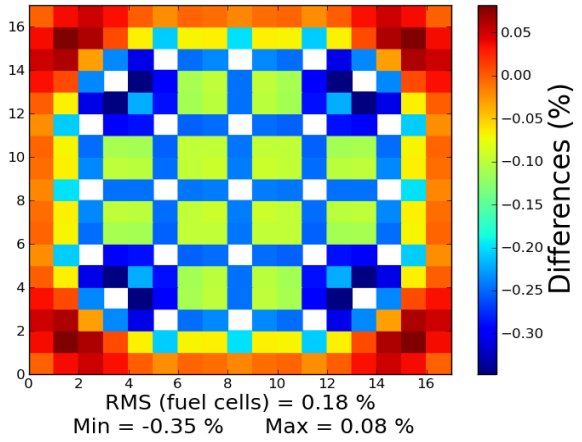

Fig. 15. Cell by cell relative power differences obtained with photon transport in a fresh UOX assembly. Guide thimbles are out of the color scale.

The third assembly which is studied is a UOX-Gd assembly with 12 pins that contain gadolinium (see Fig. 16).

The UOX-Gd assembly has a somewhat different behavior due to the presence of gadolinium. The gadolinium is a strong neutron absorber and the fission rate and then the total power deposited in pins that contain gadolinium will be much lower than in other pins. The neutron absorption will cause a significant gamma emission and the power in those pins will

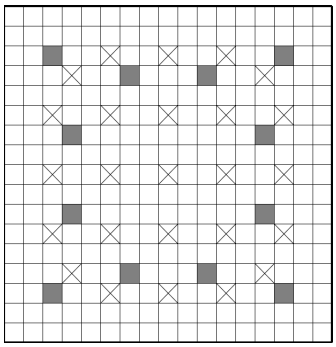

Fig. 16. UOX-GD assembly. The crosses represent the guide thimbles. Shaded cells are those that contain gadolinium.

greatly decrease ($\simeq -30\%$, see Fig. 17). The micro-depletion is however not affected in the gadolinium pins because we preserve the fission rates in those pins. The other UOX pins are just slightly affected by the gamma transport.

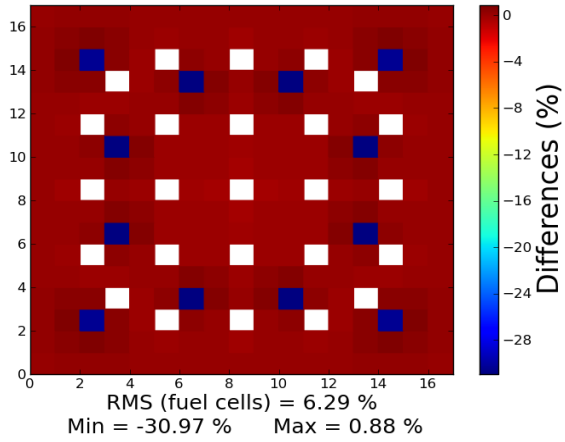

Fig. 17. Cell by cell relative power differences obtained with photon transport in a fresh UOX-Gd assembly. Guide thimbles are out of the color scale.

On the other hand, photons emitted by the gadolinium pins will be mainly absorbed by the closest pins. This explains why the power deposited in the pins neighboring the gadolinium ones will increase between 0.5% and 0.9% (see Fig. 18).

The gadolinium is consumed during depletion and after $16GWd/ton$ its effect will decrease rapidly. As a result, after a burnup of $16GWd/ton$ we observe differences in power distribution that are similar to those obtained for the UOX assembly.

The gamma transport brings large differences in the power map. The following sections of this work will show the differences brought by gamma transport on clusters and then on a core.

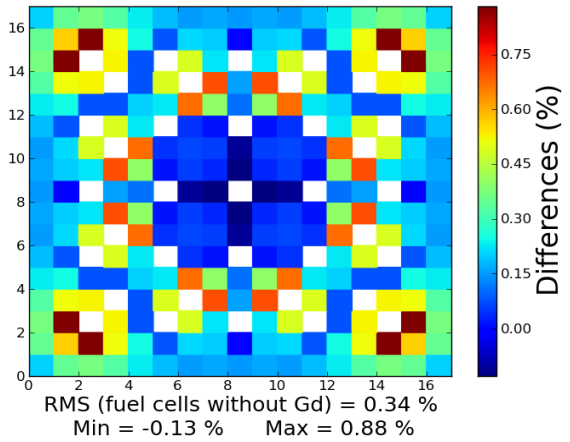

Fig. 18. Cell by cell relative power differences obtained with photon transport in a fresh UOX-Gd assembly. Guide thimbles and gadolinium pins are out of the color scale.

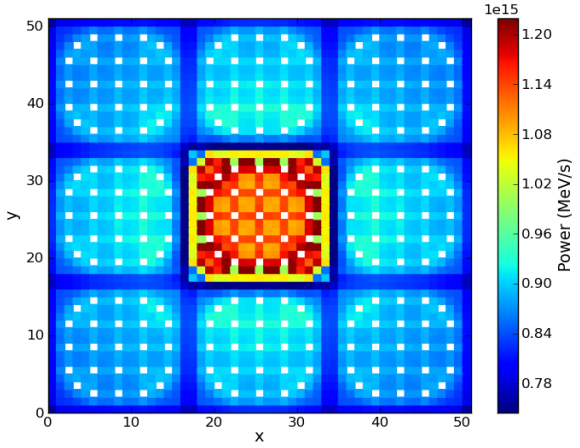

Fig. 19. Power deposited on a MOX cluster after gamma transport. Guide thimbles are out of the color scale.

2. Cluster calculations

Before considering core studies, cluster calculations were performed to study the effects of the environment on the power map and the impact of photons on it. The clusters we studied are simply made up from 9 assemblies : one of the three fresh assemblies described before, surrounded by 8 UOX assemblies already burnt at $24GWd/ton$. In this section, power maps and comparisons are obtained with REL-94 calculations with a P5 order of anisotropy. We will focus on a cluster with a MOX assembly at the center, the behavior observed for the other clusters being very similar.

First, as the fuel in the surroundings assemblies is already partially burnt, the neutron flux, the gamma flux and the powers are much larger in the center assembly. For the MOX cluster, the highly enriched MOX cells can reach $1.21MeV/s$ while the UOX cells are all lower than $0.92MeV/s$ (see Fig. 19).

Compared to the MOX assembly alone, the impacts of the gamma transport is less significant : while the relative differences were between -0.8% and 2.4%, they are now between -1.40% and 1.37% (see Fig. 20). The major changes are for the less enriched pins : after transporting photons, the power deposited in them steps up around 0.4% (2.0% to 2.4% before). With regard to the hot spots, they are logically located on highly enriched MOX pins, and they stay at the same spatial location whether or not we transport photons. In the case of this clusters, we observe that the power deposited in the hot spots decreases by 1.27%.

When we study more closely the behavior of three different types of fuel cells (one for each enrichment), it is clear that fewer photons are absorbed by the cells of the central assembly (see Fig. 21). This is because more photons are produced in the central (fresher fuel) than in the surrounding assemblies. In lattice calculations, these photons are reabsorbed in the MOX while for cluster calculations they are captured by the depleted UOX assemblies. Furthermore, this effect remains

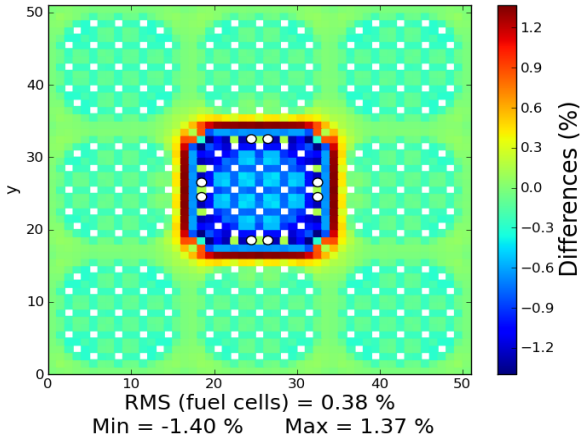

Fig. 20. Differences on the power map after transporting photons. Guide thimbles are out of the color scale. The 8 white circles represent the hot spots of this cluster.

valid for the entire depletion period.

These behaviors are also observed for UOX and UOX-Gd assemblies.

Finally, the environment of an assembly has noteworthy effects on the power maps and has to be taken into consideration particularly to study the peripheral cells of an assembly.

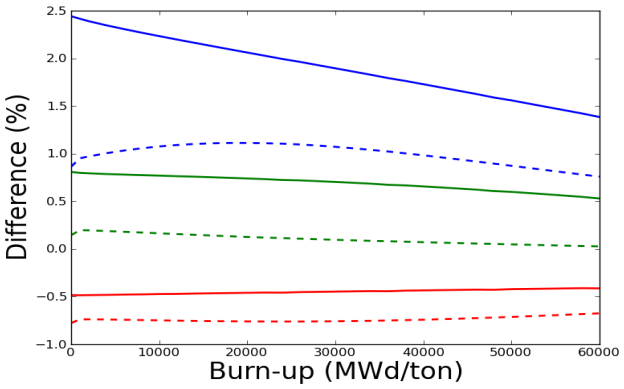

Fig. 21. Impact of the environment on 3 different cells : highly enriched cells (red), intermediate cells (green) end low enriched cells (blues). Doted lines represent the cells in a cluster. Full lines result from assembly calculations.

3. Impact of the photon transport on core calculations

The core we studied is the benchmark KAIST-1A [8]. This core is made up from 5 different assemblies (see Fig. 22).

UOX 2,00 %	UOX 2,00 %		
MOX	UOX 3,30 %	UOX 2,00 %	
UOX 3,30 %	MOX-Gd	UOX 3,30 %	UOX 2,00 %
UOX-Gd	UOX 3,30 %	MOX	UOX 2,00 %

Fig. 22. Description of a quarter of the KAIST benchmark.

We performed TRIPOLI-4 calculations with and without gamma transport as a reference. The hot spots are located at the same position with and without gamma transport. Due to the presence of gadolinium pins at the center of the core, the hot spots are located on the MOX-Gd assemblies (see Fig. 23). More precisely, the hot spots are located on low enriched pins of these assemblies. The power map also shows that the power decreases rapidly as we move away from the central assemblies and reaches 0 at the periphery of the core.

The impact of gamma transport on the power map follows a similar trend as for the clusters : the power map becomes smoother because the power deposited increases at the periphery of the core, where it was the lowest, and reduces slightly in the hottest assemblies (MOX and MOX-Gd assemblies, see Fig. 24). In the KAIST core, the gamma transport leads to a decrease of 1.58% in power at the hot spots.

We also used the 3-D reactor code COCAGNE, still in development at EDF R&D to perform core calculations. Neutron calculations with COCAGNE for KAIST-1A have already been validated by EDF [9, 10]. Our neutron-gamma core calculations use databases (cross section libraries) called DKLIB created using the schemes described before for APOLLO-2. More particularly we store in these databases normalized power maps to be able to rebuild the core power maps using homogeneous or heterogeneous calculations. We also store reaction rates allowing us to rebuild the power maps after pin-by-pin calculations. Both of these parameters (normalized power maps and reaction rates) are generated twice: once before gamma transport and once after gamma transport. So, with these databases we are able to perform homogeneous, heterogeneous and pin-by-pin calculations. To evaluate rapidly the effects of the gamma transport on full cores, diffusion calculations with 2 energy groups are performed. However, no matter what kind of calculations was performed the local relative gamma effect was always the same and was the one directly coming from the DKLIB. As a result, the effects of the environment, described before, can't be reproduced in our COCAGNE calculations. This led to some difficulties : even if the global gamma effects are similar in the TRIPOLI-4 and COCAGNE calculations, some particular pins have very different behaviors after gamma transport, including the hot spots. While the hot spots power decreased by 1.58% in TRIPOLI-4, it now increases by 0.94% (see Fig. 25).

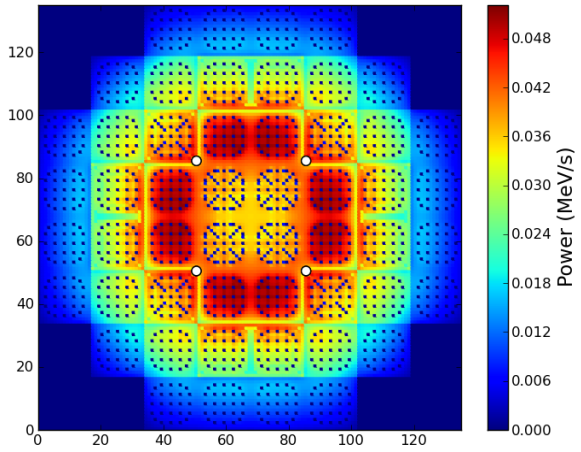

Fig. 23. Power deposited in the KAIST core after gamma transport. Results obtained from TRIPOLI-4. The hot spots are represented by the white circles and are located on low enriched pins of the MOX-Gd assemblies.

The problem of gamma transport can particularly be observed when we compare TRIPOLI-4 calculations and SP3 transport calculations with COCAGNE. Indeed, before gamma transport, the root mean square of the power differences is equal to 0.45% (see Fig. 26). After gamma transport, this root mean square increases by to 1.02% (see Fig. 27).

Moreover, it clearly appears on the Fig. 27 that the highest differences between the power maps after gamma transport

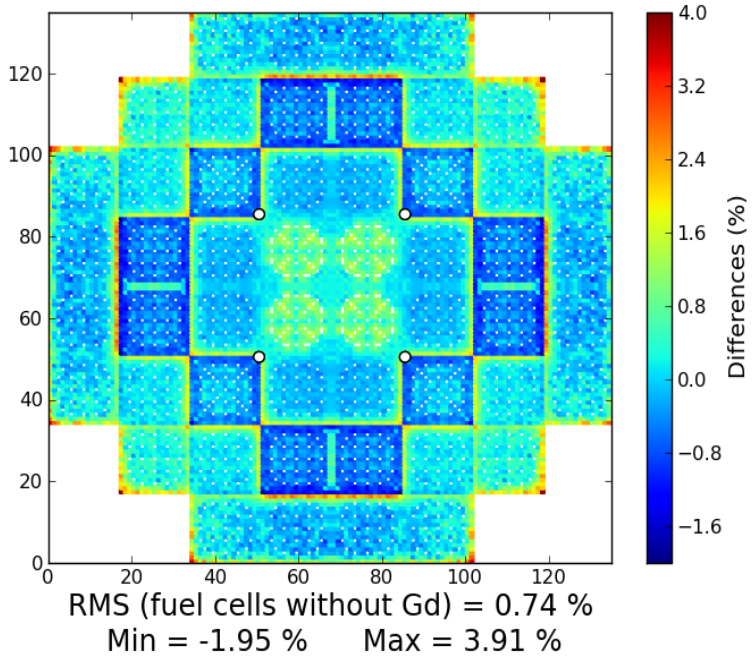

Fig. 24. Differences in the power map brought by gamma transport on KAIST-1A. Results obtained with TRIPOLI-4. Cells that contain gadolinium and guide thimbles are out of the color scale. The hot spots are represented by the white circles and are located on low enriched pins of the MOX-Gd assemblies.

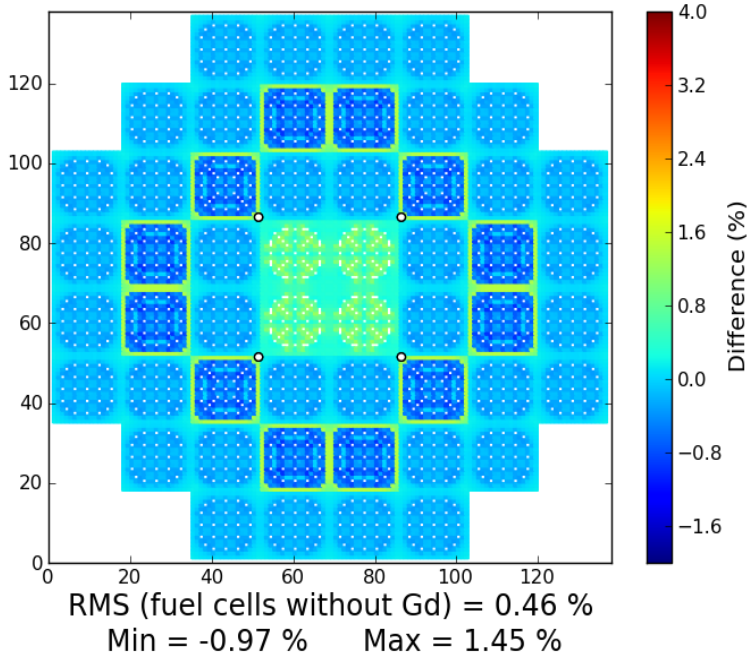

Fig. 25. Differences in the power map brought by gamma transport on KAIST-1A. Results obtained with COCAGNE. Cells that contain gadolinium and guide thimbles are out of the color scale. The hot spots are represented by the white circles and are located on low enriched pins of the MOX-Gd assemblies.

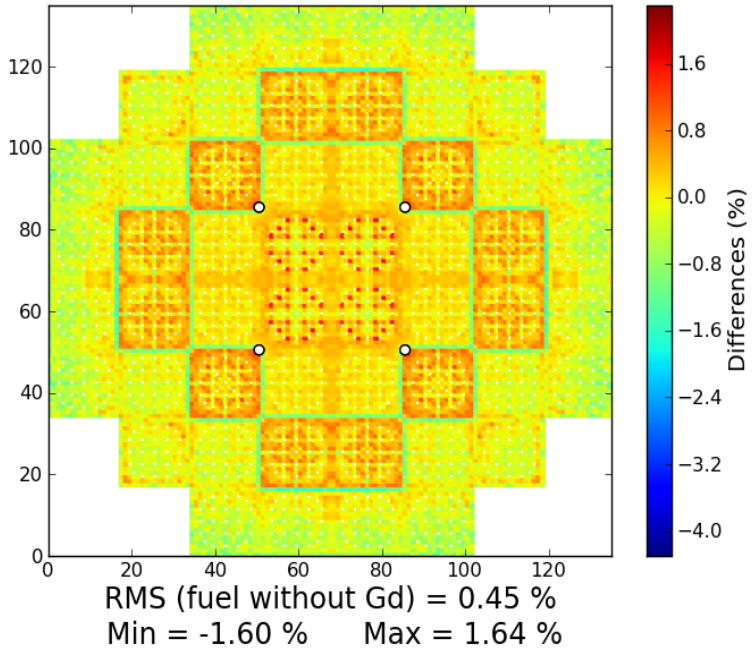

Fig. 26. Differences in the power map between TRIPOLI-4 and COCAGNE before gamma transport. Cells that contain gadolinium and guide thimbles are out of the color scale.

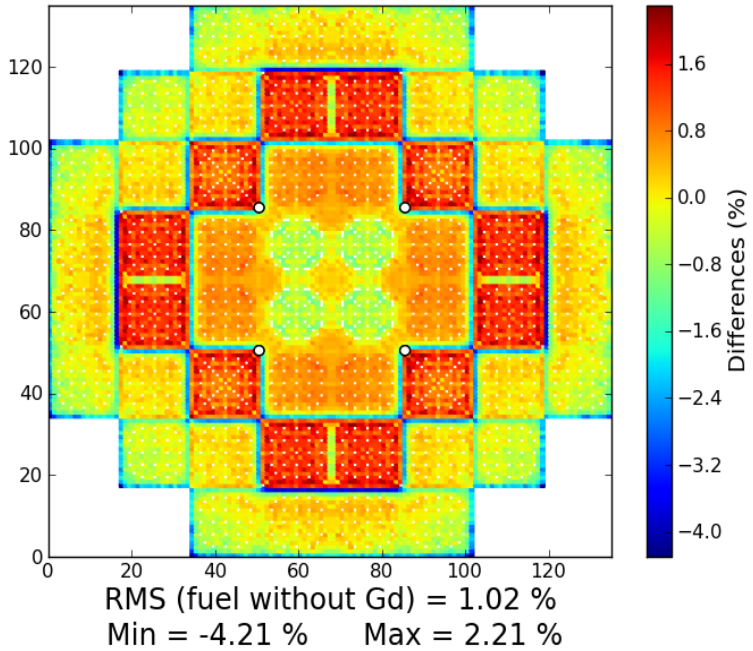

Fig. 27. Differences in the power map between TRIPOLI-4 and COCAGNE after gamma transport Cells that contain gadolinium and guide thimbles are out of the color scale.

are located in and around the MOX and MOX-Gd assemblies, where the gamma flux is the most important.

Even though we are able to use cross sections to rebuild the power on a core with COCAGNE, we are not able yet to simulate the photon transport with it. Because the mean free path of gamma photons is much higher than that of neutrons, the power deposited by photons in an assembly depends heavily on the environment. As a result, before being used, COCAGNE needs to get an additional parameter to calculate the impact of the environment on the gamma transport. Yet, it has to be noted that this benchmark is a very heterogeneous core containing only fresh assemblies where the impact of the environment is expected to be the largest.

Therefore only the global gamma transport impact can be seen with COCAGNE calculations, and this impact may not be accurately estimated for particular pins.

IV. CONCLUSIONS

We validated three deterministic neutron-gamma calculation schemes including a reference and an optimized scheme. We showed that photons can change the power deposited in UOX-Gd cells by up to 30% and above 1% on the other fuel cells. The effects of the environment on an assembly were also demonstrated to be critical, notably when the reactivity of two nearby assemblies is very different due to the change of burnup or the change of composition. Cluster calculations showed that pins at the periphery of each assembly are particularly affected. Taken as a whole, gamma transport smoothes down the global power distribution of clusters but it is important to remember that gadolinium pins have large local effects.

Finally, photons have significant consequences on power maps and particularly on the hot spots. In practice, if the gamma transport shows that the power deposited on the hot spots is underestimated in present calculation chains, the safety margins could be revalued, Conversely, if the power deposited on the hot spots is really overestimated, industries could raise the core power and still respect present safety margins. Therefore, gamma studies have great safety and economic interests and further analysis should be carried out to complete the study for nuclear cores.

V. ACKNOWLEDGMENTS

This material is based upon work supported by the Institut de Génie Nucléaire from Polytechnique Montréal in partnership with Électricité de France (EDF). Also, thanks to the CEA for the development version of APOLLO-2 that allows flux reconstruction at 281 groups for the REL94 and REL-2005-gamma schemes.

REFERENCES

1. R. SANCHEZ ET AL., "APOLLO2 YEAR 2010," *Nuclear Engineering & Technology*, **42**, *5*, 474–499 (October 2010).
2. J.-F. VIDAL, O. LITAIZE, D. BERNARD, ET AL., "New modelling of LWR assemblies using the APOLLO2 code package," in "Proceedings of Joint International Topical Meeting on Mathematics and Computations and Supercomputing in Nuclear Applications, M & C + SNA," Monterey, CA (April 2007).
3. J. RHODES, K. SMITH, D. LEE, "CASMO-5 Development and Applications," in "Proceedings of PHYSOR 2006," Vancouver, BC, Canada (September 2006).
4. AREVA NP INC., "The ARCADIA® Reactor Analysis System for PWRs Methodology Description and Benchmarking Results," Tech. rep., Areva NP Inc. (March 2010).
5. A. LUTHI, *Development and validation of gamma-heating calculational methods for plutonium-burning fast reactors*, Ph.D. thesis, École polytechnique fédérale de Lausanne (1998).
6. TRIPOLI4® PROJECT TEAM, "TRIPOLI-4® CEA, EDF and AREVA Reference Monte Carlo Code," in "Proceedings of SNA + MC 2013 - Joint International Conference on Supercomputing in Nuclear Applications + Monte Carlo," SNA+M&C 2003, Paris, France (2013).
7. E. BRUN, E. DUMONTEIL, F. X. HUGOT, N. HUOT, C. JOUANNE, Y. K. LEE, F. MALVAGI, A. MAZZOLO, O. PETIT, J. C. TRAMA, A. ZOIA, "Overview of TRIPOLI-4® version 7 Continuous-Energy Monte Carlo Transport Code," in "Proceedings of ICAPP 2011," Nice, France (2011).
8. N. Z. CHO, *KAIST Nuclear Reactor Analysis and Particle Transport Laboratory,* Benchmark Problem 1A (March 2013).
9. A. CALLOO, S. HUY, D. COUYRAS, C. BROSSELARD, M. FLISCOUNAKIS, "Validation of the SP_n depletion schemes of the EDF GABv2-COCAGNE tools using the KAIST 1A benchmark," in "Proceedings of PHYSOR 2016," Sun Valley, Idaho, USA (2016).
10. A. CALLOO, H. LEROYER, M. FLISCOUNAKIS, D. COUYRAS, "Core Neutronics Methodologies Applied to the MOX-loaded KAIST 1A benchmark: reference to industrial calculations," in "Proceedings of PHYSOR 2014," The Westin Miyako, Kyoto, Japan (October 2014).